



Photocatalytic removal of methyl orange using Ag/Zn–TiO₂ nanoparticles prepared by different methods

Robab Mohammadi^{a,*}, Mohammad Mohammadi^b

^aDepartment of Chemistry, Payame Noor University, P.O. Box: 19395-3697, Tehran, Iran, Tel. +98 411 5421414;

Fax: +98 411 5431067; email: mohammadi_rb@yahoo.com

^bFaculty of Engineering, Mechanical Engineering Department, Urmia University, Urmia, Iran, Tel. +98 441 2813202;

Fax: +98 441 4761165; email: m.mohammadi67@gmail.com

Received 11 June 2014; Accepted 8 April 2015

ABSTRACT

Ag/Zn–TiO₂ nanoparticles were synthesized via two different methods: sol–gel method in the presence of ethanol under refluxing temperature and sol–gel low-temperature route in the presence of acetic acid under 0°C. The prepared samples were characterized by X-ray diffraction, transmission electron microscopy, energy-dispersive X-ray spectroscopy, N₂ adsorption–desorption isotherm, and Brunauer–Emmett–Teller analysis methods. The effects of preparation method on the crystalline structure, crystal size, and surface area of prepared Ag/Zn–TiO₂ nanoparticles were studied. Photocatalytic activity of synthesized nanoparticles was tested by photocatalytic removal of methyl orange (MO) under UV light radiation. The effects of preparation method, initial dye concentration, and recyclability of photocatalysts were studied. Ag/Zn–TiO₂ nanoparticles prepared via sol–gel method showed high photocatalytic activity during degradation of MO under UV light radiation due to increase in the specific surface area, total pore volume, and decrease in the crystallite size.

Keywords: Ag/Zn–TiO₂ nanoparticle; Sol–gel low-temperature; Preparation method; Photocatalytic activity

1. Introduction

Large volumes of wastewater are generated in manufacturing operations by the textile dyeing industry [1]. Traditional treatment processes such as micellar enhanced ultrafiltration, cation-exchange membranes, adsorption/precipitation processes, integrated chemical–biological degradation, integrated iron (III) photoassisted-biological treatment, solar photo-Fenton and biological processes cannot efficiently degrade the synthetic dyes. A popular process

which has high potential to control environmental pollutants is heterogeneous photocatalysis [2,3]. Among different semiconductors, Titania nanoparticles have received much interest due to its high photochemical stability, low cost, lack of toxicity, and strong photocatalytic activity [4]. However, photocatalytic activity is low because of recombination of photo-generated electron–hole pairs [5]. In order to increase its efficiency, titanium dioxide is doped with different metal oxides and ions [6]. Photogenerated electrons can be trapped by dopants and electron–hole recombination is prevented. There are many reports in the case of doping metal ions which can increase the

*Corresponding author.

photocatalytic efficiency of TiO₂. Saha et al. [7] reported the impregnation of commercial TiO₂ with silver nanoparticles at 1 and 2 mol% Ag using a simple “liquid impregnation followed by heat treatment” method. In order to study the effect of silver impregnation, they investigated UV-induced photodegradation of malachite green (MG) using prepared photocatalyst. They found that the presence of silver in TiO₂ increases the photon-induced mineralization of MG but decreases the decolorization efficiency. Co-doping metal ions into the undoped TiO₂ is a suitable way to increase the activity of TiO₂ [8]. Segne et al. [9] prepared TiO₂ nanocatalyst co-doped with magnesium and copper. They reported that co-doping of Mg²⁺/Cu²⁺ into TiO₂ shifts the absorbance band of TiO₂ from UV to visible region and the band gap energy is reduced for co-doped catalyst (from 3.2 to 2.50 eV). Based their results, the photocatalytic degradation of methylene blue over the catalyst surface of nano co-doped Mg²⁺/Cu²⁺ TiO₂ was higher than over undoped TiO₂. Estrellan et al. [10] presented photocatalytic decomposition of perfluorooctanoic acid by iron and niobium co-doped titanium dioxide. They concluded that Fe:Nb–TiO₂ has the highest activity compared to the undoped TiO₂ and the commercially available TiO₂ which related to the influences of co-doping both on the physico-chemical properties and surface interfacial charge transfer mechanisms.

Since photoactivity of TiO₂ is directly related to its morphology [11], all the oxidation reactions and photocatalysis take place on the surface of TiO₂. Furthermore, the photodegradation efficiency depends on the various parameters such as the number of catalytic surface active sites, surface area of the photocatalyst, the source of light, and other structural properties. Since these properties can be improved via tailoring the shape and dimensionality, the size and shape control of TiO₂ is an important parameter for accessing to the most applications of this photocatalyst [12]. Although there are a variety of reports on different preparation route of TiO₂, however, a comparative investigation to emphasize the influence of the different methods on the properties of the samples has not been yet reported. Herein, we report the preparation of anatase TiO₂ via simple and inexpensive routes such as sol–gel and sol–gel low-temperature methods. The purpose of this research work was to compare the properties of the products with each other and to study the relationship between photocatalyst structure, crystal size, specific surface area, and photocatalytic activity. We also investigate the effect of Ag and Zn dopants on the photoactivity of samples. The effect of various parameters such as pollutant concentration and recyclability of Ag/Zn–TiO₂ nanoparticles were studied.

2. Materials and methods

2.1. Materials

Titanium *n*-butoxide (TBOT, Ti(OC₄H₉)₄) was used as starting material. Ethanol with absolute grade, glacial acetic acid, zinc nitrate, and silver nitrate were used without any further purification. Methyl orange (MO) was used as a model pollutant to measure the photocatalytic activity of synthesized samples. All chemicals used in this work were supplied from Merck (Germany).

2.2. Sample preparation

2.2.1. Preparation of Ag/Zn–TiO₂ nanoparticles via sol–gel method in the presence of ethanol under reflux temperature

According to Behnajady et al. [13], for the synthesis of TiO₂ nanoparticles, titanium *n*-butoxide was slowly dissolved in absolute ethanol. Then, distilled H₂O was added drop by drop into a flask containing TBOT/EtOH mixture under reflux and magnetic stirring. The molar ratio of TBOT/EtOH/H₂O was 1:1:65. The yellowish transparent sol was yielded after continuously stirring for 3 h. Then, TiO₂ xerogel was calcined at 450°C for 3 h and TiO₂ nanoparticles were yielded. Ag/Zn–TiO₂ nanoparticles were synthesized by the same method, except that the water used for the synthesis contained the required amount of AgNO₃ and Zn(NO₃)₂. The components of mixed solution are listed in Table 1 (given as molar ratio of doping silver and zinc).

2.2.2. Preparation of Ag/Zn–TiO₂ via sol–gel low-temperature method in the presence of acetic acid under 0°C

According to Behnajady et al. [14], in order to prepare TiO₂ nanoparticles by sol–gel low-temperature method, titanium *n*-butoxide was slowly dissolved in

Table 1
*k*_{obs} values for different photocatalysts in the photocatalytic removal of MO

Catalyst	Ag:Zn	<i>k</i> _{obs}
TiO ₂	0:0	0.059
Ag–TiO ₂	0.01:0	0.098
Ag–TiO ₂	0.03:0	0.13
Ag–TiO ₂	0.06:0	0.163
Ag–TiO ₂	0.09:0	0.181
Ag–TiO ₂	0.1:0	0.174
Zn–TiO ₂	0:0.01	0.081
Ag/Zn–TiO ₂	0.09:0.01	0.219
Ag/Zn–TiO ₂	0.09:0.02	0.242
Ag/Zn–TiO ₂	0.09:0.03	0.228

glacial acetic acid (AcOH). After stirring for 5 min at 0°C, distilled water was added drop by drop to the above solution under vigorous stirring conditions. The molar ratio of TBOT/AcOH/H₂O was 1:1:200. The homogeneous solution was yielded after continuously stirring for 1 h. Then, the obtained sol–solution was kept in darkness for 12 h for nucleation process. Obtained solution was placed in an air oven at 70°C for gelation procedure. The gel was then dried at 100°C for overnight. Finally, the dry gel powder was calcined at 450°C for 3 h. Ag/Zn–TiO₂ nanoparticles (Ag 0.09 mol %, Zn 0.02 mol%) were prepared via the same method, except that the water used for the preparation contained the required amount of AgNO₃ and Zn(NO₃)₂.

2.3. Characterization of Ag/Zn–TiO₂ nanoparticles

The crystal phase composition and the crystallite size of Ag/Zn–TiO₂ nanoparticles were recorded using X-ray diffraction (XRD) (Siemens/D5000) with CuK α radiation (0.15478 nm) in the 2 θ scan range of 15–70°. The structure and size of the prepared samples were investigated using transmission electron microscope (Philips CM-10 HT-100 kV). The chemical composition of the prepared catalysts was analyzed by an EDX system. BET measurement was performed using Belsorp mini II instrument based on N₂ adsorption–desorption isotherms.

2.4. Photocatalytic degradation procedures

Photocatalytic removal of MO was conducted in a batch quartz reactor. All photocatalytic experiments were applied at ambient temperature and atmospheric pressure. Artificial illumination was provided by 15 W (UV-C) with a wavelength peak at 254 nm, which positioned above to the reactor. In each run, desired concentration of Ag/Zn–TiO₂ nanoparticles (400 mg L⁻¹) and MO was fed into the quartz tube reactor and placed in the dark condition for 30 min with continuous stirring for adsorption–desorption equilibrium and then exposed to UV light irradiation [15]. Every 3 min as interval time, a sample was withdrawn and centrifuged to remove catalyst particles, and the concentration of MO was determined by UV–Vis Perkin-Elmer 550 SE spectrophotometer at wavelengths of 465 nm.

3. Results and discussion

3.1. Characterization of Ag/Zn–TiO₂ nanoparticles

3.1.1. X-ray diffraction

The phase composition and the crystallite size of the synthesized samples were investigated by XRD

analysis. The XRD patterns of Ag/Zn–TiO₂ powders (Ag 0.09 mol%, Zn 0.02 mol%) synthesized by sol–gel and sol–gel low-temperature methods are illustrated in Fig. 1(a) and (b), respectively. All the peaks in the XRD patterns can be indexed as anatase phases of Ag/Zn–TiO₂. The average crystal size was obtained by Debye–Scherrer's formula given by following equation [16]:

$$D = \frac{k\lambda}{\beta \cos \theta} \quad (1)$$

where D is the crystal size; λ is the wavelength of the X-ray radiation ($\lambda = 0.15406$ nm) for CuK α ; K is usually taken as 0.89; and β is the line width at half-maximum height [17]. The crystallite size obtained using this formula is 9 nm for sol–gel derived particles and 16.5 nm in case of sol–gel low-temperature method-derived particles. For both samples, Ag and Zn species were not detected. It is related to low metal loading as well as appropriate dispersion of metal ions on TiO₂ crystal structure [18].

3.1.2. TEM analysis of prepared nanoparticles

TEM images provide adequate evidences to investigate the morphology and the size of the

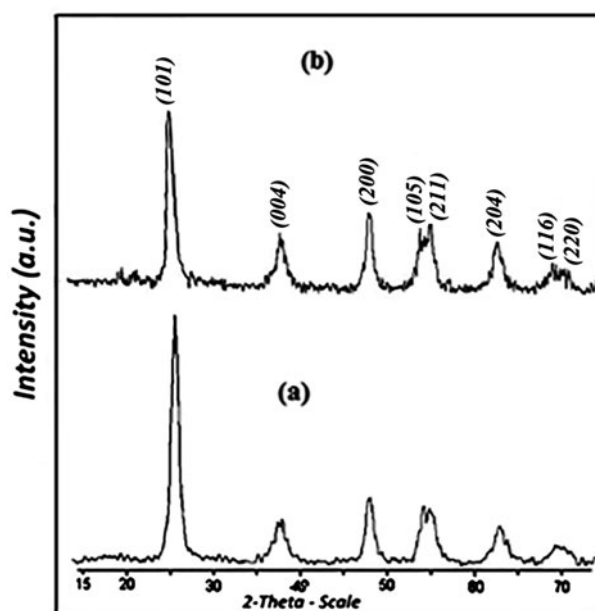


Fig. 1. XRD patterns of Ag/Zn–TiO₂ nanoparticles prepared by (a) sol–gel and (b) sol–gel low-temperature methods.

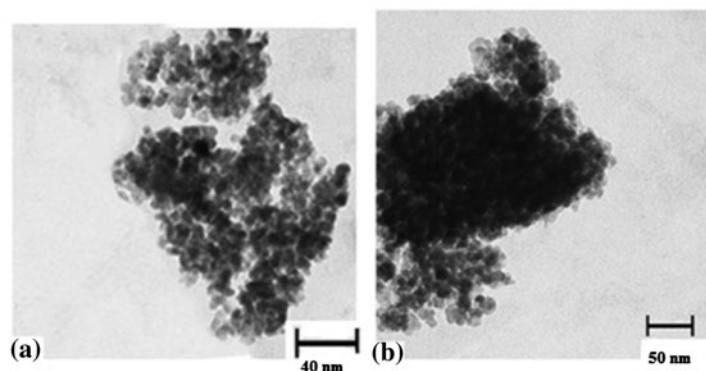


Fig. 2. TEM images of Ag/Zn-TiO₂ nanoparticles prepared by (a) sol-gel and (b) sol-gel low-temperature methods.

samples. TEM image of Ag/Zn-TiO₂ nanoparticles (Ag 0.09 mol%, Zn 0.02 mol%) prepared by sol-gel method is illustrated in Fig. 2(a). Clear global structure can be observed in TEM image. The mean size of nanoparticles is estimated to be about 7–10 nm. Fig. 2(b) shows TEM image of Ag/Zn-TiO₂ nanoparticles prepared by sol-gel low-temperature method. Agglomeration of sol-gel low-temperature derived nanopowders is higher than that of sol-gel derived nanopowders. As can be seen from the TEM image, the average particle size is 14–18 nm. The crystallite size of Ag/Zn-TiO₂ nanoparticles prepared by sol-gel method is less than that of Ag/Zn-TiO₂ nanoparticles prepared by sol-gel low-temperature method. This difference in crystallite size could be ascribed to the little aggregation of the nanoparticles obtained by sol-gel method. The TEM results were in good agreement with that calculated from the XRD pattern using Scherrer equation.

3.1.3. Elemental analysis with energy-dispersive X-ray spectroscopy (EDX):

The EDX data of Ag/Zn-TiO₂ nanoparticles (Ag 0.09 mol%, Zn 0.02 mol%) prepared by sol-gel method are illustrated in Fig. 3. TiO₂ shows a peak around 0.5 keV, and another intense peak appears at 4.5 keV. The intense peak is assigned to TiO₂ in the bulk form, and the less intense peak is assigned to TiO₂ surface [19]. The existence of Ag⁺ and Zn²⁺ ions in the solid catalyst can be confirmed by these results. Detection of metals in very low content with this analysis method is because of appropriate and uniform distribution of metals.

3.1.4. BET analysis

Fig. 4 shows nitrogen adsorption-desorption isotherms of Ag/Zn-TiO₂ nanoparticles (Ag 0.09 mol%,

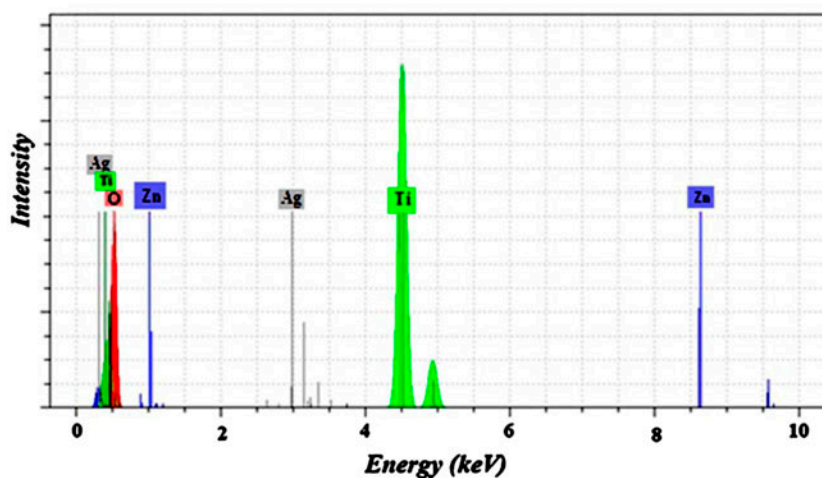


Fig. 3. EDX patterns of Ag/Zn-TiO₂ nanoparticles prepared by sol-gel method.

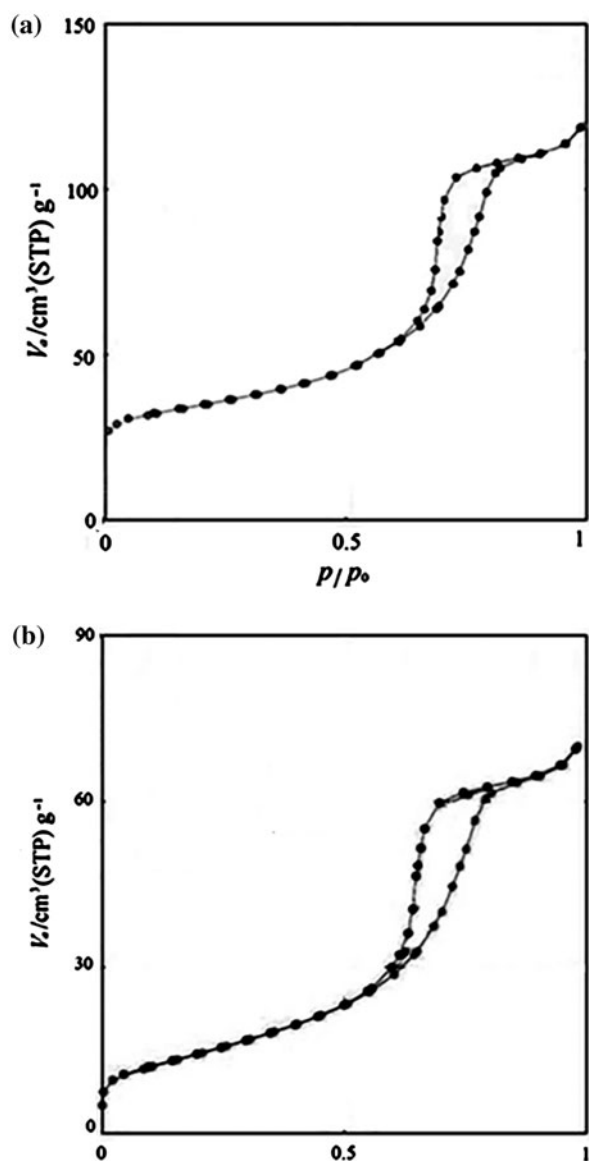


Fig. 4. N_2 adsorption–desorption isotherms of Ag/Zn- TiO_2 nanoparticles prepared by (a) sol-gel and (b) sol-gel low-temperature methods.

Zn 0.02 mol%) prepared by sol-gel and sol-gel low-temperature methods. Both samples show type IV isotherms. At high relative pressures from 0.55 to 0.85, the shape of hysteresis loop is of type H2, implying the existence of an ink bottle-type pores structure with narrow necks and wide bodies, indicating that the particles contain mesopores because of the aggregation of crystallites [20]. The porous structure can help to transport of reactant molecules and products through the interior space because of the interconnected porous frameworks and favor the harvesting of light

because of large surface area and multiple scattering within the porous network [21].

BET surface area and total pore volume for sol-gel derived nanopowders (Ag 0.09 mol%, Zn 0.02 mol%) were $98.61 \text{ m}^2 \text{ g}^{-1}$ and $0.185 \text{ cm}^3 \text{ g}^{-1}$, respectively, which is higher than $61.5 \text{ m}^2 \text{ g}^{-1}$ and $0.127 \text{ cm}^3 \text{ g}^{-1}$ of sol-gel low-temperature derived sample. The increased surface area of sol-gel derived nanopowders compared to sol-gel low-temperature-derived sample is due to its increase in the mesopore size and mesopore volume [22]. It is known that heterogeneous photocatalysis is affected mainly by surface area and pore structure. Higher surface area and pore volume is a main factor in the formation of photogenerated electron-hole pairs.

3.2. Photocatalytic activity of prepared samples

The semi-logarithmic graph of the concentration of MO in the presence of different photocatalysts vs. UV light illumination time yield straight lines, which confirm the pseudo-first-order kinetics for removal of MO in this procedure. The pseudo-first-order rate constant (k_{obs}) for photocatalytic removal of MO was obtained from slope of the semi-logarithmic graphs. Table 1 summarizes all the obtained k_{obs} for removal of MO in the presence of different samples.

Results in this table show that Ag-Zn/ TiO_2 photocatalyst containing 0.09 mol% Ag and 0.02 mol% Zn has better photocatalytic activity than TiO_2 , Ag/ TiO_2 , and Zn/ TiO_2 in the removal of MO. Results in Table 1 indicate that k_{obs} is increased significantly with increasing in silver doping up to 0.09 mol%. Direct calcination of the nanopowders containing Ag ions can enable formation of Ag particles up 400°C via thermal decomposition procedure [23]. Ag-doped TiO_2 can indirectly modify the interfacial charge transfer processes and also act as an efficient electron scavenger [24]. The Fermi levels of Ag is lower than the CB of TiO_2 [25]. Therefore, photoexcited electrons can be transferred from the CB of titanium dioxide to silver particles deposited on its surface, while photo-generated VB holes stay on the photocatalyst. Accumulated electrons on silver particles and holes on TiO_2 can be used to carry out the reduction and oxidation reaction, respectively. While holes on the photocatalyst can be used to carry out the oxidation reaction. So, recombination of photogenerated electron-hole can be prevented by doping of metals with suitable work-function, which useful for higher photocatalytic activity.

However, Ag content more than 0.09 mol% lead to decrease in the activity of photocatalyst due to

following reasons: Reducing of active sites on the photocatalyst surface in order to contact and adsorb of dye and other species such as hydroxyl ions, decrease of photogenerated $e^- - h^+$ pairs because of screening the TiO_2 surface from light absorption aggregation of silver particles and decrease of homogeneous distribution of dopant, and also the negatively charged Ag sites can act as a recombination center [26,27].

Results in Table 1 also show the effect of zinc dopant concentration on photocatalytic activity of Ag/ TiO_2 in the fixed silver content at optimum value (0.09 mol%). From this figure, the photoactivity is enhanced with doping of small amount of zinc (0.02 mol%), but when the amount of Zn was more than 0.02 mol%, the photocatalytic activity reduced significantly. Zn similar to Ag because of lower Fermi level than TiO_2 can capture the photoinduced electrons. While at high zinc doping, the excessive Zn species act as a significant center for electron-hole recombination [28]. Lower optimum value for Zn in the co-doped system can be attributed to the existence of silver in the adjacent of zinc. It is known that ionic radius of impregnated metal ion is a main factor influences photocatalytic activity of TiO_2 [29]. The impregnated metal ions with higher ionic radius than Ti^{4+} (such as Ag) in the interstitial positions are more useful in photoactivity than the metal ions with ionic radius close to Ti^{4+} (such as Zn) which can occupy the substitutional positions. The impregnated metal ions in the interstitial positions cause better charge separation and less electron-hole recombination. According to these investigations, Ag in the interstitial positions and Zn in the substitutional positions can separately capture photoproducted electrons and inhibit electron-hole recombination and consequently improve photoactivity.

3.2.1. Effect of preparation method on the photocatalytic activity of Ag/Zn- TiO_2 nanoparticles

The preparation method of Ag/Zn- TiO_2 nanoparticles was assigned as an important factor which can affect the efficiency of photocatalyst. From Fig. 5, the photocatalytic activity of Ag/Zn- TiO_2 nanoparticles (Ag 0.09 mol%, Zn 0.02 mol%) prepared by sol-gel method is higher than that of Ag/Zn- TiO_2 nanoparticles prepared by sol-gel low-temperature method. It is known that photoactivity of photocatalyst depends on the crystalline size, surface area, total pore volume, and morphology of sample [30]. Particle size is a main parameter influencing photocatalytic efficiency, since the electron-hole recombination rate may depend on

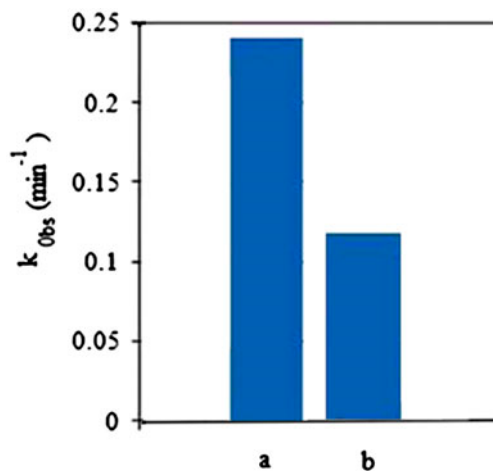


Fig. 5. Photocatalytic removal of MO in the presence of Ag/Zn- TiO_2 nanoparticles prepared by (a) sol-gel and (b) sol-gel low-temperature methods.

the particle size [31,32]. Partial variations in particle sizes lead to significant modifications in the surface/bulk ratio, thus influencing the recombination rates of volume and surface electrons and holes [33]. Sol-gel-derived nanoparticles with small particle size can decrease the electron-hole recombination rate. Furthermore, higher degradation efficiency of sol-gel-derived nanoparticles could be related to larger surface area and total pore volume compared to another sample. Large specific surface area allows more dyes to be absorbed onto the surface of Ag/Zn- TiO_2 nanoparticles, while high pore volume (mesopores) allows fast diffusion of different liquid reactants and products during the photocatalytic reaction, which can enhance the rate of photocatalytic degradation [34,35]. The results revealed that the sol-gel method for preparation of TiO_2 nanoparticles can produce photocatalyst with better activity.

3.2.2. Kinetic study as function of initial dye concentration

The influence of initial dye concentration was investigated in the range of 10–40 $mg L^{-1}$. The plot of $\ln(C_0/C)$ vs. time for all the tests with various dye concentration is shown in Fig. 6. The values of k_{obs} can be obtained by applying a least square regression analysis. As can be seen from Fig. 7, the value of k_{obs} is decreased by increasing initial dye concentration. This behavior can be due to following reasons:

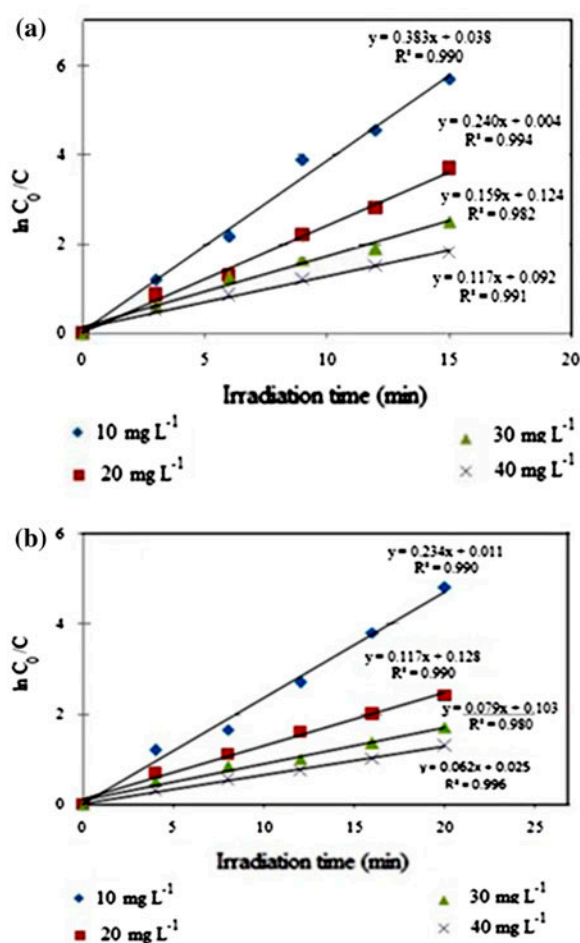


Fig. 6. Determination of the pseudo-first-order kinetic rate constant, k_{obs} : (a) sol-gel and (b) sol-gel low-temperature methods.

- With increasing of dye concentration, more and more pollutant molecules are adsorbed on the surface of Ag/Zn-TiO₂ nanoparticles. Therefore, the generation of active species such as $\cdot\text{OH}$ will be decreased [36].
- With increasing of dye concentration, the solution becomes impermeable to UV radiation because the molar extinction coefficient of MO at wavelength of UV light (254 nm) is very high; therefore, the photons get intercepted before they can reach Ag/Zn-TiO₂ nanoparticles surface [37].

Classic Langmuir-Hinshelwood (L-H) mechanism can be applied to explain the kinetic of the photocatalytic removal of most organic dyes which in terms of degradation kinetics can be described as follows [38]:

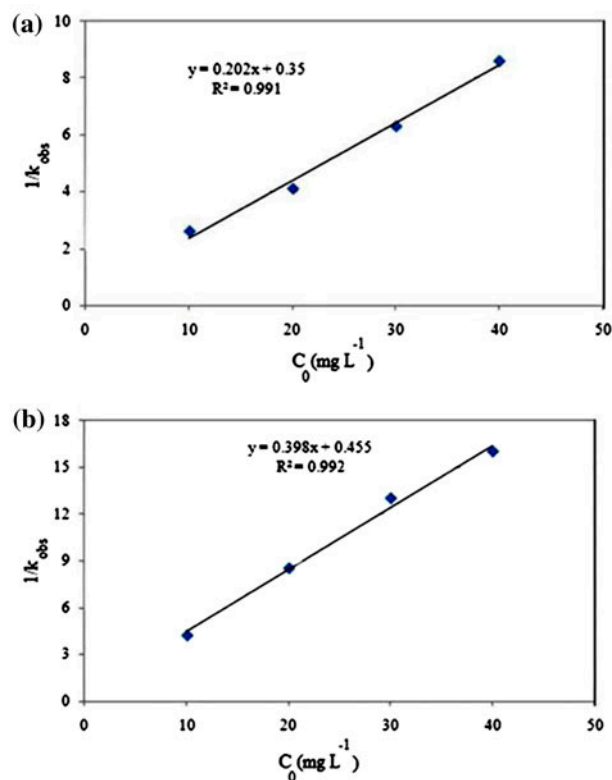


Fig. 7. Determination of the adsorption equilibrium constant, k_{dye} , and the second-order rate constant, k_C , for the Langmuir-Hinshelwood kinetic model: (a) sol-gel and (b) sol-gel low-temperature methods.

$$r = \frac{k_C k_{dye}(C)}{1 + k_{dye}(C_0)} \quad (2)$$

$$\frac{1}{k_{obs}} = \frac{1}{k_C k_{dye}} + \frac{C_0}{k_C} \quad (3)$$

In these equations, k_{dye} and k_C are the adsorption equilibrium constant and surface reaction rate constant, respectively. k_{dye} and k_C can be calculated using the resulted data from photocatalytic tests with different initial dye concentrations and plotting $1/k_{obs}$ vs. C_0 . A straight line fitted the experimental data indicates that photodegradation of MO follows Langmuir-Hinshelwood kinetics (Fig. 7). From the slope and the intercept of this line, k_C and k_{dye} were computed. Table 2 reports the values of k_C and k_{dye} for both samples resulting from plot of $\frac{1}{k_{obs}}$ vs. " C_0 ".

3.2.3. Recycling of Ag/Zn-TiO₂ nanoparticles

In order to investigate whether Ag/Zn-TiO₂ nanoparticles (Ag 0.09 mol%, Zn 0.02 mol%) can be

Table 2

k_{dye} and k_{C} values in photocatalytic removal of MO by prepared samples

	k_{C}	k_{dye}
Sol-gel derived nanoparticles	4.95	0.577
Sol-gel low-temperature derived nanoparticles	2.51	0.875

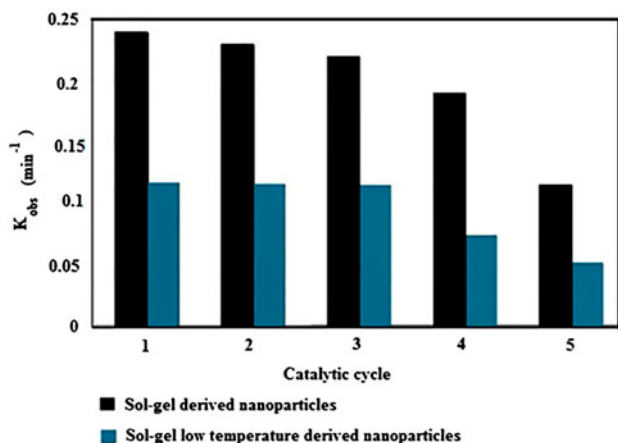


Fig. 8. Catalytic yields of 400 mg L⁻¹ of Ag/Zn-TiO₂ as a function of its reuse of 20 mg L⁻¹ of MO photocatalytic removal.

reused after photodegradation, Ag/Zn-TiO₂ nanoparticles were used and recycled for consecutive reuse on MO removal. The reaction was repeated up to five times, and the efficiency of the process was investigated and compared between the reuse cycles. From Fig. 8, Ag/Zn-TiO₂ nanoparticles demonstrated good stability after recovery. As can be seen that, after three cycles, the efficiency markedly decreased. Agglomeration and sedimentation of MO molecules around Ag/Zn-TiO₂ nanoparticles after each cycle of photocatalytic reaction is a possible reason of the observed decline on the photocatalytic activity, because each time Ag/Zn-TiO₂ nanoparticles are reused new parts of photocatalysts surface become unavailable for pollutant adsorption and thus photon absorption, reducing the efficiency of the photocatalyst.

4. Conclusions

We have successfully prepared Ag/Zn-TiO₂ nanoparticles by different methods. Structure and morphology of samples were characterized using various techniques. The crystal size, surface area, and pore volume strongly were affected by preparation

method. The experimental results showed that photocatalytic activity of Ag/Zn-TiO₂ nanoparticles prepared by sol-gel method is more than that of Ag/Zn-TiO₂ nanoparticles prepared by sol-gel low-temperature method. The recycling of both samples can be carried out with the photocatalyst being able to be adequately used in other reactions. Based on this research work, we conclude that better crystallinity, high-specific surface area, and the morphology correlate with the photocatalytic activity. As technical advantages, this study provides an approach for highly efficiency method to synthesize high active anatase photocatalyst.

Acknowledgment

We thank the Payame Noor University I.R. of Iran for supporting this research.

References

- [1] A.R. Khataee, M.B. Kasiri, Photocatalytic degradation of organic dyes in the presence of nanostructured titanium dioxide: Influence of the chemical structure of dyes, *J. Mol. Catal. A: Chem.* 328 (2010) 8–26.
- [2] R. Vijayalakshmi, V. Rajendran, Synthesis and characterization of nano-TiO₂ via different methods, *Arch. Appl. Sci. Res.* 4 (2012) 1183–1190.
- [3] S.F. Aquino, C.A. Lacerda, D.R. Ribeiro, Use of ferrites encapsulated with titanium dioxide for photodegradation of azo dyes and color removal of textile effluents, *Environ. Eng. Sci.* 27 (2010) 1049–1059.
- [4] K.M. Lee, V. Suryanarayanan, K.C. Ho, Influences of different TiO₂ morphologies and solvents on the photovoltaic performance of dye-sensitized solar cells, *J. Power Sources* 188 (2009) 635–641.
- [5] E.D. Jeong, P.H. Borse, J.S. Jang, J.S. Lee, O.S. Jung, H. Chang, J.S. Jin, M.S. Won, H.G. Kim, Hydrothermal synthesis of Cr and Fe co-doped TiO₂ nanoparticle photocatalyst, *J. Ceram. Process. Res.* 9 (2008) 250–253.
- [6] C. Chen, Z. Wang, S. Ruan, B. Zou, M. Zhao, F. Wu, Photocatalytic degradation of C.I. acid orange 52 in the presence of Zn-doped TiO₂ prepared by a stearic acid gel method, *Dyes Pigm.* 77 (2008) 204–209.
- [7] S. Saha, J.M. Wang, A. Pal, Nano silver impregnation on commercial TiO₂ and a comparative photocatalytic account to degrade malachite green, *Sep. Purif. Technol.* 89 (2012) 147–159.
- [8] R. Parra, L.A. Ramajo, M.S. Góes, J.A. Varela, M.S. Castro, From tin oxalate to (Fe Co, Nb)-doped SnO₂: Sintering behavior, microstructural and electrical features, *Mater. Res. Bull.* 43 (2008) 3202–3211.
- [9] T.A. Segne, S.R. Tirukkavalluri, S. Challapalli, Studies on characterization and photocatalytic activities of visible light sensitive TiO₂ nano catalysts Co-doped with magnesium and copper, *Int. Res. J. Pure Appl. Chem.* 1 (2011) 84–103.
- [10] C.R. Estrellan, C. Salim, H. Hinode, Photocatalytic decomposition of perfluorooctanoic acid by iron and niobium co-doped titanium dioxide, *J. Hazard. Mater.* 179 (2010) 79–83.

- [11] X.H. Xia, Y. Liang, Z. Wang, J. Fan, Y.S. Luo, Z.J. Jia, Synthesis and photocatalytic properties of TiO₂ nanostructures, *Mater. Res. Bull.* 43 (2008) 2187–2195.
- [12] T. Yunxiang, L. Yong, J. Miao, Phase transformation in NiTiHf shape memory alloy thin films, *Thin Solid Films* 516 (2008) 5393–5396.
- [13] M.A. Behnajady, H. Eskandarloo, N. Modirshahla, M. Shokri, Investigation of the effect of sol-gel synthesis variables on structural and photocatalytic properties of TiO₂ nanoparticles, *Desalination* 278 (2011) 10–17.
- [14] M.A. Behnajady, H. Eskandarloo, N. Modirshahla, M. Shokri, Sol-gel low-temperature synthesis of stable anatase-type TiO₂ nanoparticles under different conditions and its photocatalytic activity, *Photochem. Photobiol.* 87 (2011) 1002–1008.
- [15] R. Mohammadi, B. Massoumi, M. Rabani, Photocatalytic decomposition of amoxicillin trihydrate antibiotic in aqueous solutions under UV irradiation using Sn/TiO₂ nanoparticles, *Int. J. Photoenergy*, ID 514856 (2012) 1–11.
- [16] M. Hamadani, A. Reisi-Vanani, A. Majedi, Sol-gel preparation and characterization of Co/TiO₂ nanoparticles: Application to the degradation of methyl orange, *J. Iran. Chem. Soc.* 7 (2010) S52–S58.
- [17] J.G. Yu, J.C. Yu, W.K. Ho, Effects of alcohol content and calcination temperature on the textural properties of bimodally mesoporous titania, *Appl. Catal. A* 255 (2003) 309–320.
- [18] C.R. Estrellan, C. Salim, H. Hinode, Photocatalytic decomposition of perfluorooctanoic acid by iron and niobium co-doped titanium dioxide, *J. Hazard. Mater.* 179 (2010) 79–83.
- [19] T.M.L. Goerne, M.A.A. Lemus, V.A. Morales, E.G. López, P.C. Ocampo, Study of bacterial sensitivity to Ag-TiO₂ nanoparticles, *J. Nanomed. Nanotechnol.* S5-003 (2012) 1–7, doi: 10.4172/2157-7439.S5-003.
- [20] J. Fang, H. Bao, B. He, F. Wang, D. Si, Z. Jiang, Z. Pan, S. Wei, W. Huang, Interfacial and surface structures of CeO₂-TiO₂ mixed oxides, *J. Phys. Chem. C* 111 (2007) 19078–19085.
- [21] P. Madhusudan, J. Ran, J. Zhang, J. Yu, G. Liu, Novel urea assisted hydrothermal synthesis of hierarchical BiVO₄/Bi₂O₃CO₃ nanocomposites with enhanced visible-light photocatalytic activity, *Appl. Catal. B* 110 (2011) 286–295.
- [22] F. Dumeignil, K. Sato, M. Imamura, N. Matsubayashi, E. Payen, H. Shimada, Characterization and hydrodesulfurization activity of CoMo catalysts supported on sol-gel prepared Al₂O₃, *Appl. Catal., A: General* 287 (2005) 135–145.
- [23] M.K. Seery, R. George, P. Floris, S.C. Pillai, Silver doped titanium dioxide nanomaterials for enhanced visible light photocatalysis, *J. Photochem. Photobiol. A: Chem.* 189 (2007) 258–263.
- [24] R. Georgekutty, M.K. Seery, S.C. Pillai, A highly efficient Ag-ZnO photocatalyst: Synthesis, properties, and mechanism, *J. Phys. Chem. C* 112 (2008) 13563–13570.
- [25] V. Subramanian, E.E. Wolf, P.V. Kamat, Catalysis with TiO₂/gold nanocomposites. Effect of metal particle size on the fermi level equilibration, *J. Am. Chem. Soc.* 126 (2004) 4943–4950.
- [26] O. Carp, C.L. Huisman, A. Reller, Photoinduced reactivity of titanium dioxide, *Prog. Solid State Chem.* 32 (2004) 33–177.
- [27] R. Mohammadi, B. Massoumi, Sn/Cu-TiO₂ nanoparticles produced via sol-gel method: Synthesis, characterization, and photocatalytic activity, *Russ. J. Phys. Chem. A* 88 (2014) 1184–1190.
- [28] N. Venkatachalam, M. Palanichamy, B. Arabindoo, V. Murugesan, Synthesis and characterization of zirconium-doped mesoporous nano-crystalline TiO₂, *Nanoscale* 2 (2010) 1222–1228.
- [29] R.J. Tayade, R.G. Kulkarni, R.V. Jasra, Photocatalytic degradation of aqueous nitrobenzene by nanocrystalline TiO₂, *Ind. Eng. Chem. Res.* 45 (2006) 922–927.
- [30] J. Li, J. Xu, W.L. Dai, H. Li, K. Fan, Direct hydro-alcohol thermal synthesis of special core-shell structured Fe-doped titania microspheres with extended visible light response and enhanced photoactivity, *Appl. Catal. B* 85 (2009) 162–170.
- [31] J.H. Huang, P.Y. Hung, S.F. Hu, R.S. Liu, Improvement efficiency of a dye-sensitized solar cell using Eu³⁺ modified TiO₂ nanoparticles as a secondary layer electrode, *J. Mater. Chem.* 20 (2010) 6505–6511.
- [32] B. Ahmmad, Y. Kusumoto, M.S. Islam, One-step and large scale synthesis of non-metal doped TiO₂ microspheres and their photocatalytic activity, *Adv. Powder Technol.* 21 (2010) 292–297.
- [33] X. Sun, H. Liu, J. Dong, J. Wei, Y. Zhang, Preparation and characterization of Ce/N-Codoped TiO₂ particles for production of H₂ by photocatalytic splitting water under visible light, *Catal. Lett.* 135 (2010) 219–225.
- [34] D. Jose, C.M. Sorensen, S.S. Rayalu, K.M. Shrestha, K.J. Klabunde, Au-TiO₂ nanocomposites and efficient photocatalytic hydrogen production under UV-visible and visible light illuminations: A comparison of different crystalline forms of TiO₂, *Int. J. Photoenergy* (2013) 10 (Article ID 685614).
- [35] R. Mohammadi, B. Massoumi, H. Eskandarloo, Preparation and characterization of Sn/Zn/TiO₂ photocatalyst for enhanced amoxicillin trihydrate degradation, *Desalin. Water Treat.* 53 (2015) 1995–2004.
- [36] N. Barka, S. Qourzal, A. Assabbane, Y. Ait-Ichou, Kinetic modeling of the photo-catalytic degradation of methyl orange by supported TiO₂, *J. Environ. Sci. Eng.* 4 (2010) 1–4.
- [37] M.A. Behnajady, H. Eskandarloo, Preparation of TiO₂ nanoparticles by the sol-gel method under different pH conditions and modeling of photocatalytic activity by artificial neural network, *Res. Chem. Intermed.* 41 (2015) 1327–1335.
- [38] R. Marandi, M.E. Olya, B. Vahid, M. Khosravi, M. Hatami, Kinetic modeling of photocatalytic degradation of an azo dye using nano-TiO₂/polyester, *Environ. Eng. Sci.* 29 (2012) 957–963.